Electronic supplementary information for: Heteroleptic Tethered NHC Rare Earth Initiators for the Ring Opening Polymerisation of *rac*-Lactide

Joseph W. Walker,[a] Tajrian Chowdhury,[b] Georgina M. Rosair,[a] Joy H. Farnaby,[b] Stephen M. Mansell[a] and Ruaraidh D. McIntosh[a]

a. Institute of Chemical Sciences, Heriot-Watt University, Edinburgh EH14 4AS, UK; E-mail: S.Mansell@hw.ac.uk, R.Mcintosh@hw.ac.uk
b. School of Chemistry, University of Glasgow, Joseph Black Building, Glasgow, G12 8QQ, UK

Table of Contents

Experimental details and NMR spectra

Starting materials were used as received from Acros Organics, Alfa Aesar and Thermo Scientific. All NMR spectra were collected on a Bruker AVIIIHD 400 MHz spectrometer at 298 K at Heriot Watt University. All manipulations were carried out under a dry, oxygen-free dinitrogen atmosphere using standard Schlenk line techniques or in an MBRAUN UNIlab glovebox. ^{1}H NMR spectra were recorded at 400 MHz and referenced to the residual solvent peak, 7.24 ppm for $CDCl_3$ and 7.16 ppm for C_6D_6. $^{13}C\{^{1}H\}$ NMR spectra were recorded at 101 MHz and referenced to the residual solvent peak, 128.62 ppm for C_6D_6. The Size Exclusion Chromatography analysis of polymers was carried using a Shimadzu High Performance Liquid Chromatograph fitted with a 7.5 mm internal diameter Agilent GPC column. The detector used was a Shimadzu RID-20A. HPLC grade tetrahydrofuran (THF, 99.8%, Acros Organics, Geel, Belgium) was utilized as the eluent with flow rate of 1 mL/min with an oven temperature of 30°C. The measurement was calibrated against ten polystyrene standards in the range of 162–364,000 g/mol and corrected using the Mark–Houwink parameters, PLA (K = 0.0549, α = 0.639) and PS (K = 0.0125, α = 0.717).[1] Tetrahydrofuran (THF), acetonitrile and toluene were obtained from an MBRAUN SP-300 solvent purification system; further to this, toluene was boiled over molten sodium, then collected and stored over activated 4 Å molecular sieves. Diethyl ether was received previously dried in an AcroSeal bottle and was transferred to a new vessel over 4 Å molecular sieves, residual gasses were then removed *via* 3 freeze-pump-thaw cycles. ^{n}BuLi was titrated 3 times with menthol and 2,2'-bipyridine. Elemental analyses were performed by Orla McCullough at the London Metropolitan University, using a Flash 2000 Organic Elemental Analyzer, Thermo Scientific analyser. The samples for the measurements were prepared using V2O5 (to ensure complete combustion of all complexes) in tin capsules inside an inert argon glovebox atmosphere. Deuterated benzene was stirred over molten potassium and vacuum transferred prior to use. Compound **LH_2Br** was synthesised as previously described.[2] $Ln\{N(SiMe_3)_2\}_3$ (Ln = Y, La, Ce, Nd) were synthesised from the reaction of anhydrous $LnCl_3$ salts with $NaN(SiMe_3)_2$ in THF, followed by toluene extraction and crystallisation.[3] *rac*-Lactide (Acros) was purified by recrystallisation from toluene followed by triple sublimation prior to use. Complex **1** was synthesised as previously described.[4] Complex **8** was synthesised as previously described.[5]

^{1}H NMR spectrum obtained from NMR scale reaction between CeN"$_3$ and LH_2Br (**3**)

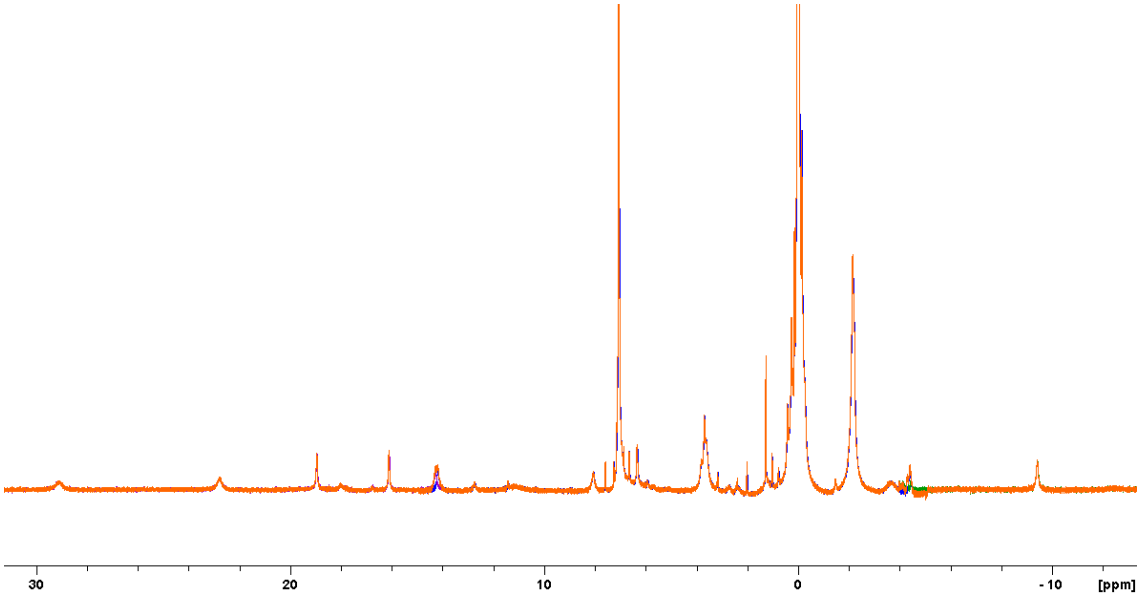

Figure S1. Merged ^{1}H NMR (400.1 MHz, 298K, C_6D_6) spectra from different sweep regions (35 – 15 ppm, 15 – -5 ppm and -5 – -25 ppm) for the reaction of CeN"$_3$ and LH_2Br after 4 days at 80 °C.

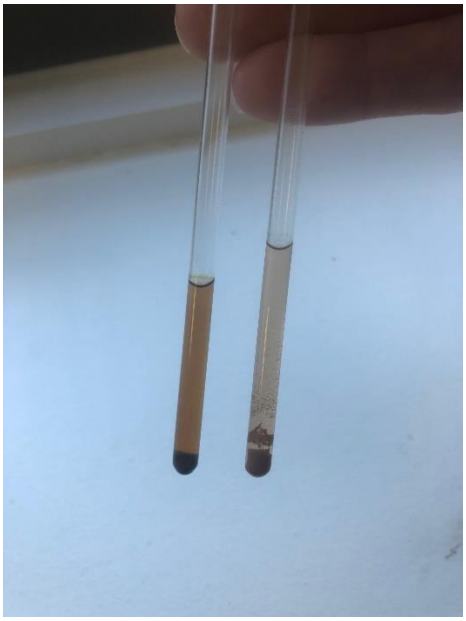

Figure S2. Attempts to redissolved **3** (LHS J. Young NMR tube) and **4** (RHS J. Young NMR tube) in d_8-THF revealed them to be very poorly soluble precluding the collection of NMR spectroscopic data on the isolated compounds.

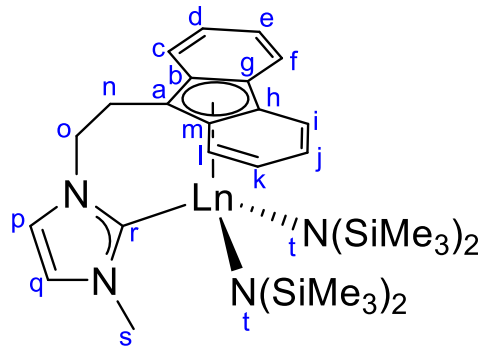

LaLN"$_2$ (**5**)

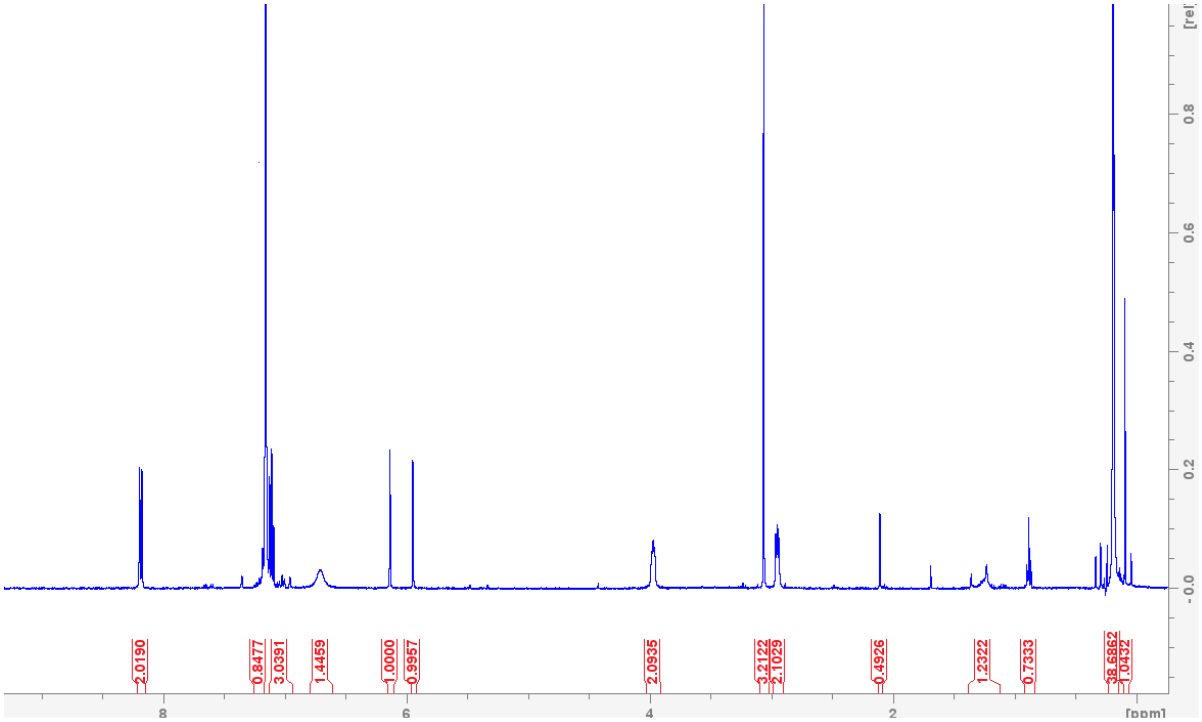

Figure S3. ^{1}H NMR (400.1 MHz, 298K, C_6D_6) spectrum of **5**.

^{1}H NMR (400.1 MHz, 298K, C_6D_6) δ /ppm: 8.27 (d, J_{HH} = 8.00 Hz 2H, H_f & H_i), 7.26-6.95 (m, 6H, H_c-H_f + H_i-H_l), 6.71 (br. s, 2H, H_e & H_j), 6.14 (d, J_{HH} = 1.62 Hz 1H, H_q), 5.95 (d, J_{HH} = 1.59 1H, H_r), 3.97 (m, 2H, H_o), 3.06 (s, 3H, H_s), 2.95 (m, 2H, H_n), 0.19 (s, 36H, H_t).

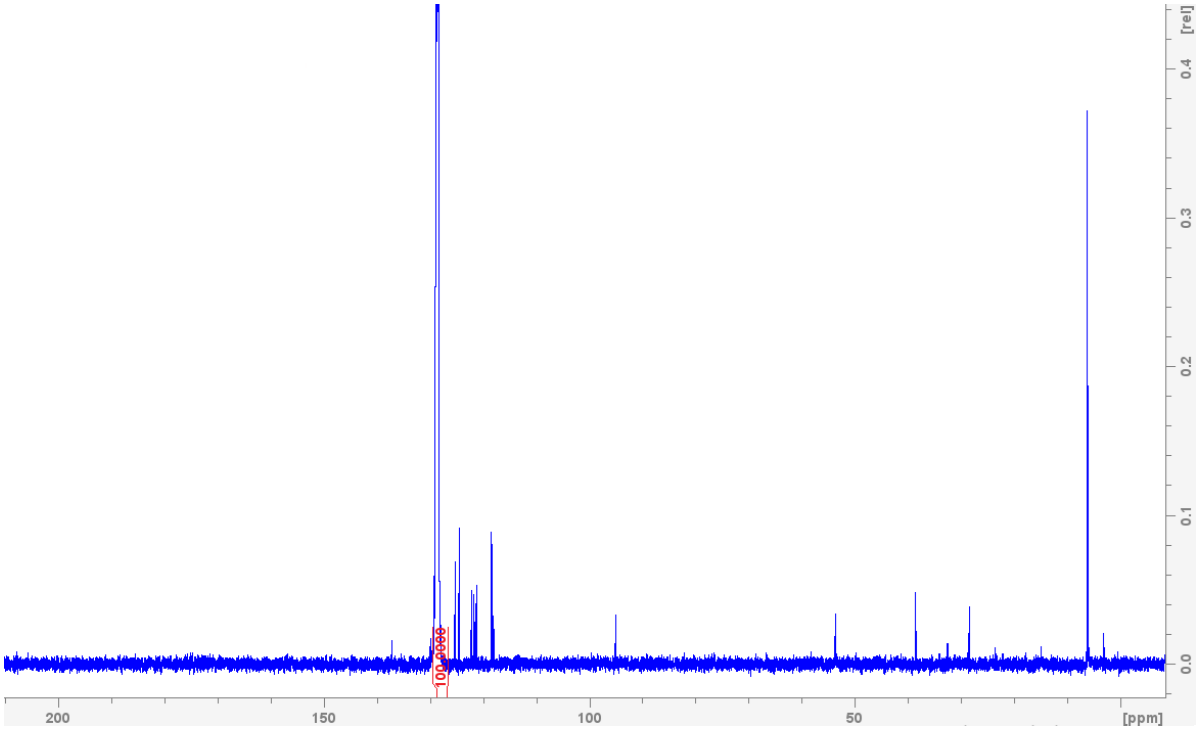

Figure S4. $^{13}C\{^{1}H\}$ NMR (101 MHz, 298K, C_6D_6) spectrum of **5**.

CeLN"$_2$(**6**)

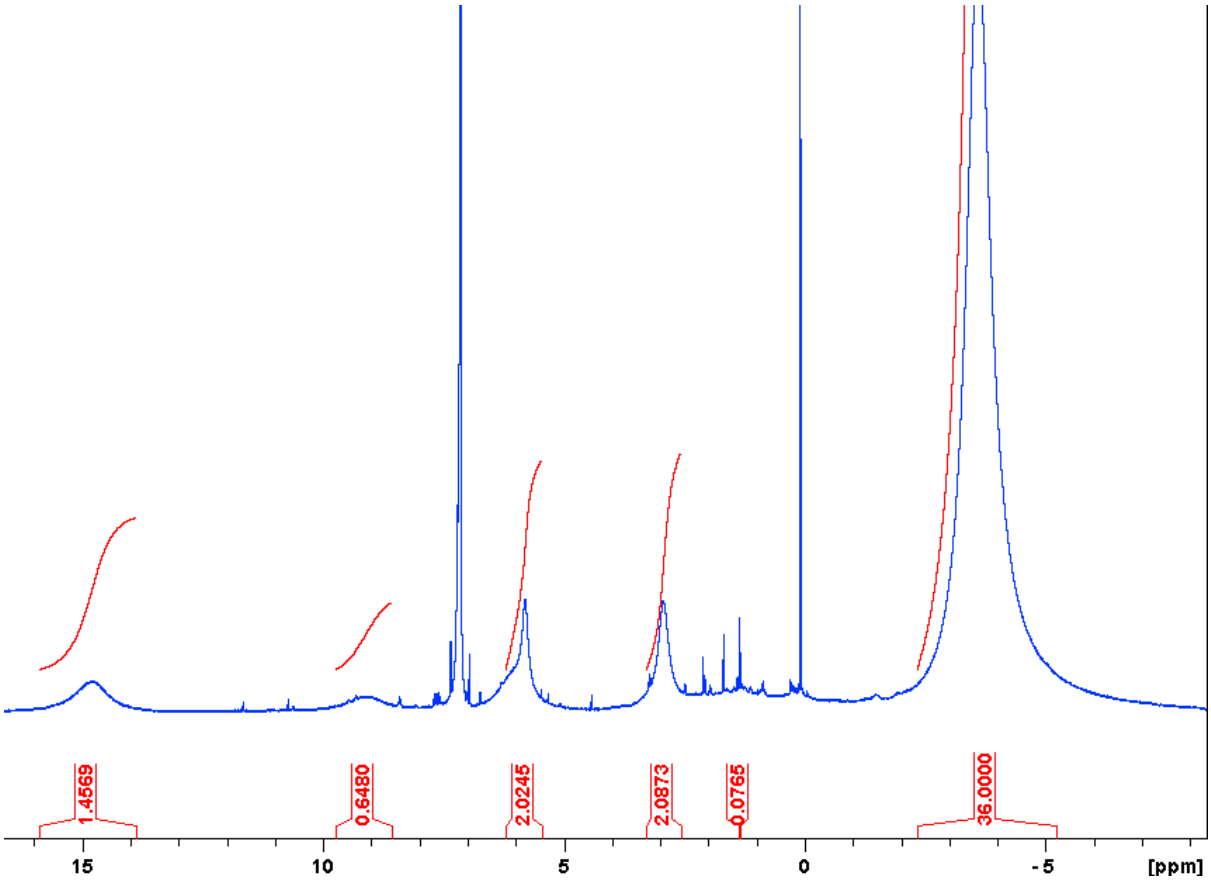

Figure S5. ^{1}H NMR (400.1 MHz, 298K, C_6D_6) of **6.** Additional peak at 0 ppm is from residual HN".

NdLN"$_2$(**7**)

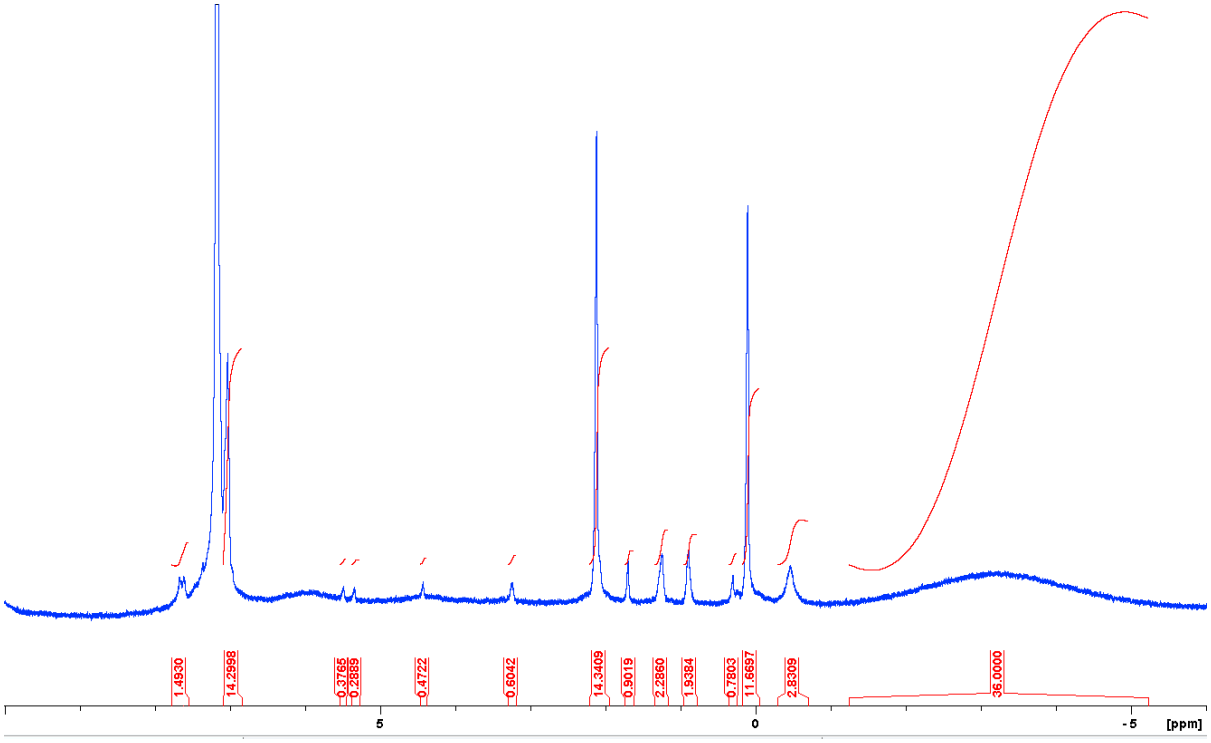

Figure S6. ^{1}H NMR (400.1 MHz, 298K, C_6D_6) of **7**. Additional peaks are from trace $HN(SiMe_3)_2$ and solvent: 0.11 ppm (s, 12H, HN"), 2.11 ppm (s, 14H, toluene).

Incomplete reaction between YN"$_3$ and LH with comparison to free LH

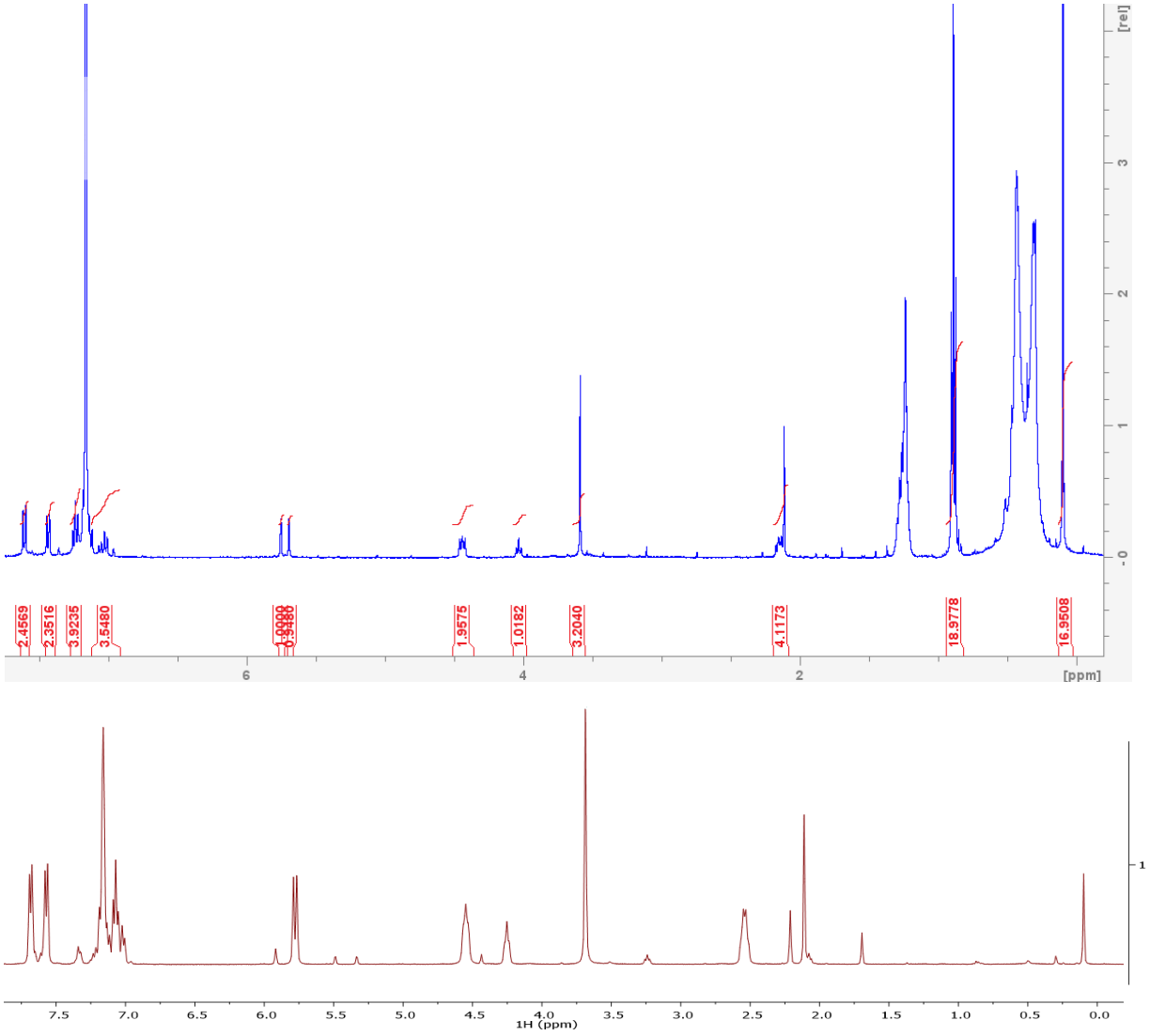

Figure S7. ^{1}H NMR (400.1 MHz, 298K, C_6D_6) spectrum of incomplete reaction between YN"$_3$ and LH (free carbene, C_6D_6 with n-hexane at 1.24 ppm, 0.89 ppm, top) and comparison with the reaction of LH_2Br + LiN" to form the free carbene LH (bottom). This shows that the free fluorene-tethered carbene has been formed not the anticipated yttrium complex.

Methine region of polymerisation reaction mixture after completion

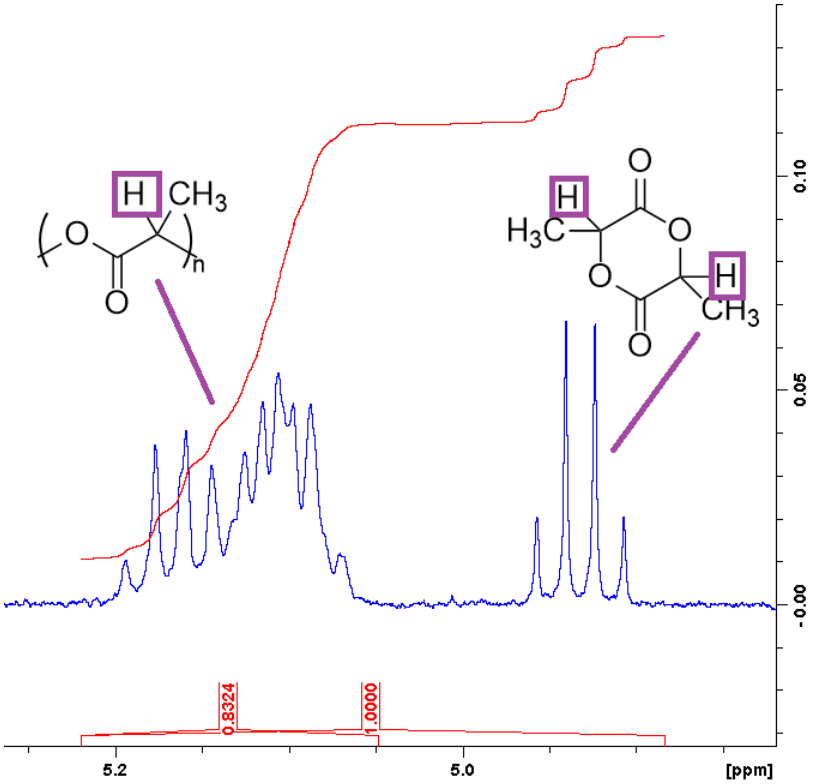

Figure S8. ^{1}H NMR spectrum (400 MHz, $CDCl_3$, 298 K) methine region of an example crude reaction mixture after completion. The distinct quartet shows the C-H from unreacted *rac*-lactide while the multiplet shows the same proton in the polymer. Integration of the two peaks is used to determine conversion, in this case conversion is 83%.

Contaminated *rac*-lactide

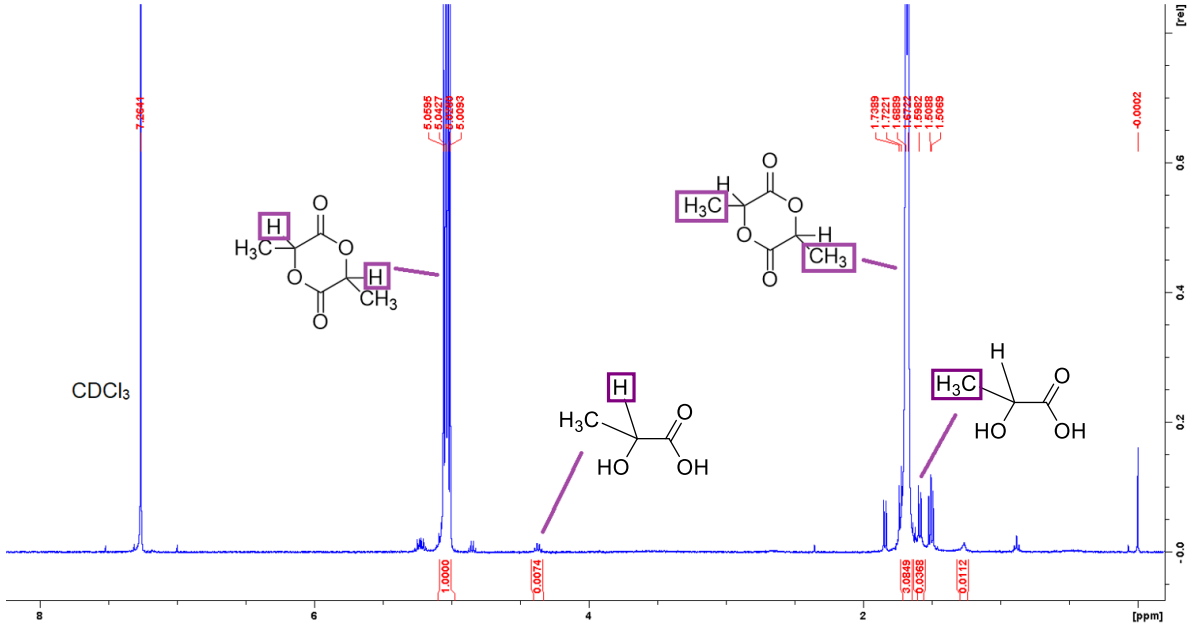

Figure S9. ^{1}H NMR spectrum (400 MHz, $CDCl_3$, 298 K) of *rac*-lactide contaminated with lactic acid (Thermo Sci) – Not used for polymerisation experiments.

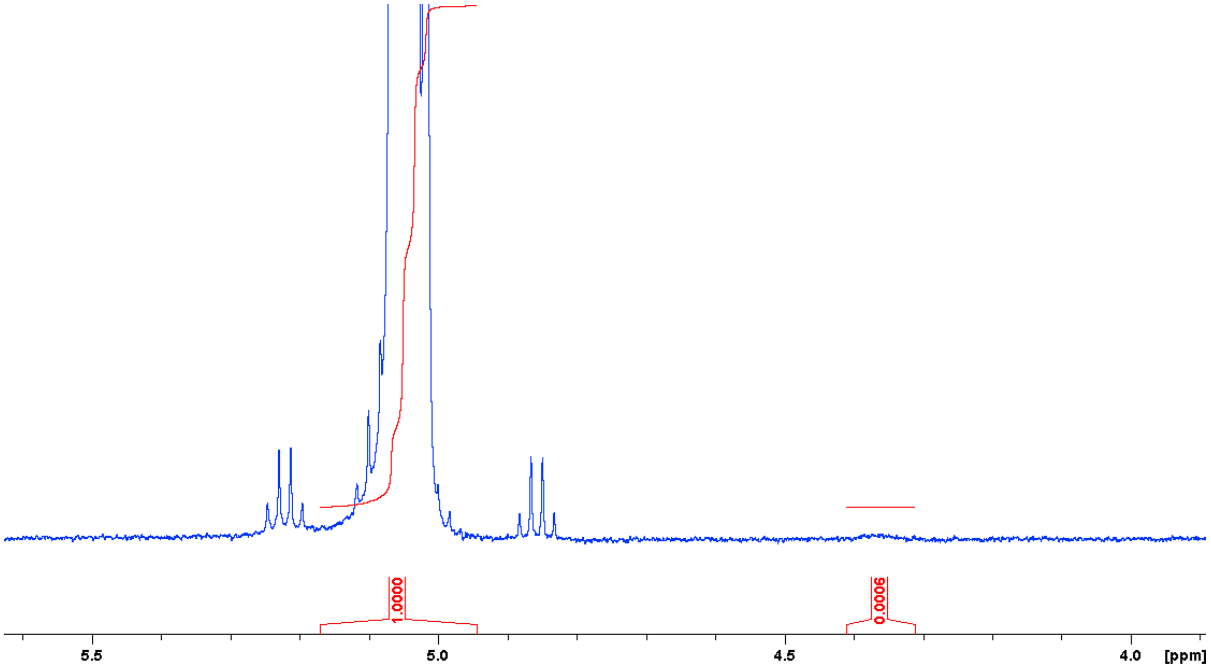

Figure S10. ^{1}H NMR spectrum (400 MHz, $CDCl_3$, 298 K) of *rac*-lactide with only negligible contamination by lactic acid (Acros) – Used for polymerisation experiments.

^{1}H NMR spectrum of reaction between YLN"Br (**1**) and BnOH

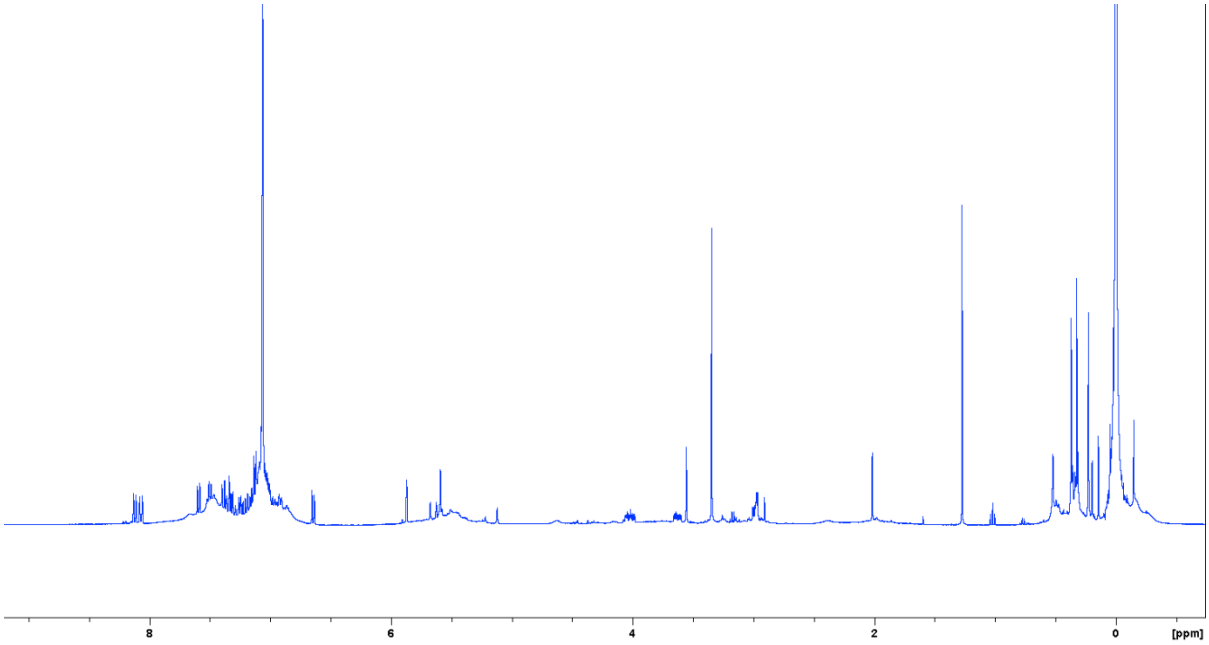

Figure S11. ^{1}H NMR (400.1 MHz, 298K, C_6D_6) spectrum of reaction between **1** and BnOH after 5 hours at room temperature

GPC traces

Measurements were calibrated against ten polystyrene standards in the range of 162–364,000 g/mol and corrected using the Mark–Houwink parameters, PLA (K = 0.0549, α = 0.639) and PS (K = 0.0125, α = 0.717). Traces are shown up to 20 minutes, at which point molecular weights are of a negligible quantity indicating completion of the run.

YLN"Br

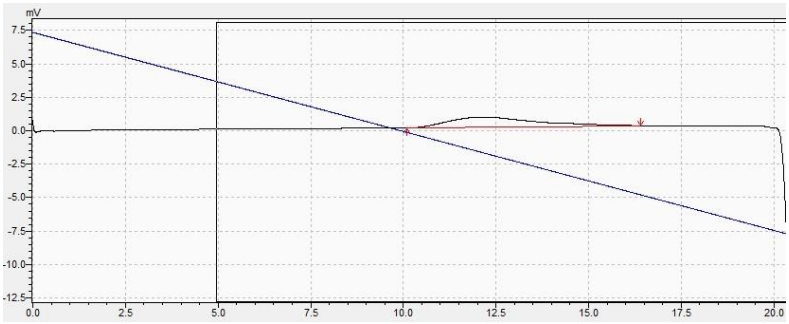

Figure S12. GPC trace for polymer product with YLN"Br (200:1, RT, 15 mins) as catalyst (Table 1, entry 1)

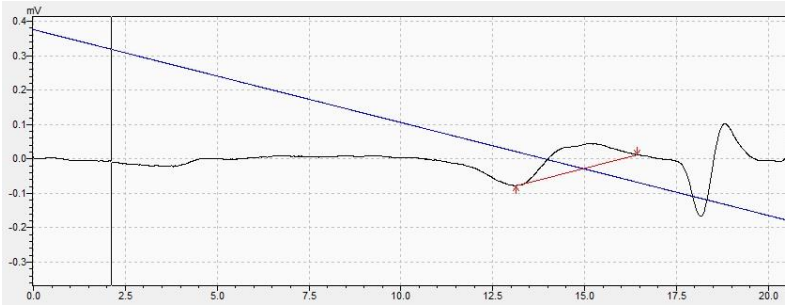

Figure S13. GPC trace for polymer product with YLN"Br (200:1, RT, 10 mins) as catalyst (Table 1, entry 2)

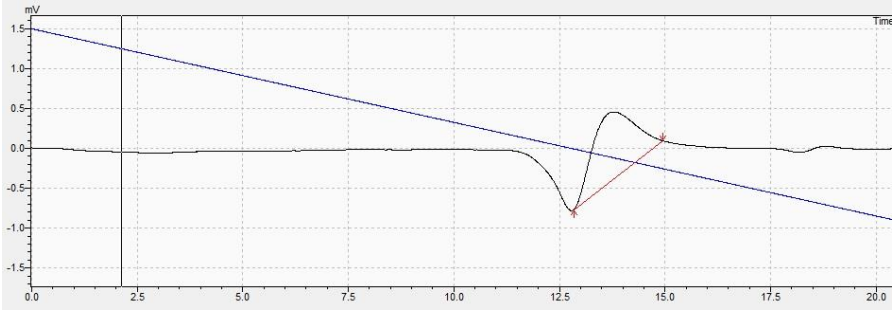

Figure S14. GPC trace for polymer product with YLN"Br (400:1, RT, 20 mins) as catalyst (Table 1, entry 3)

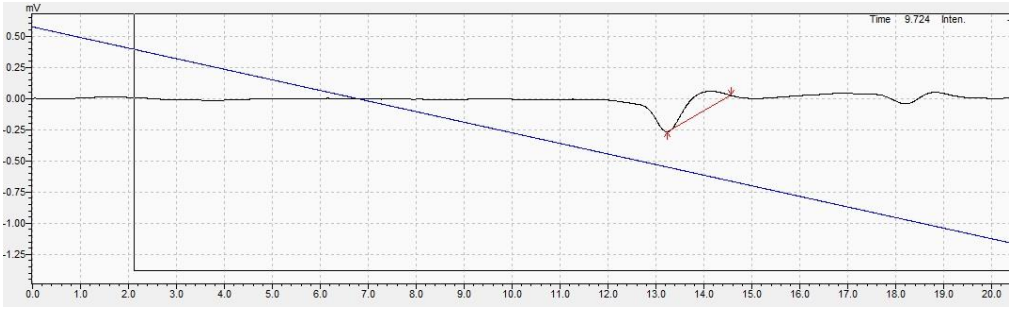

Figure S15. GPC trace for polymer product with YLN"Br (800:1, RT, 30 mins) as catalyst (Table 1, entry 4)

LaL_2Br

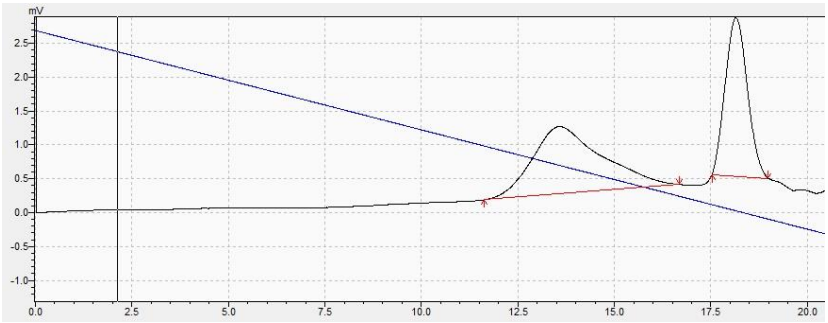

Figure S16. GPC trace for polymer product with LaL_2Br (200:1, RT, 15 mins) as catalyst (Table 1, entry 5)

$(CeLN"Br)_2$

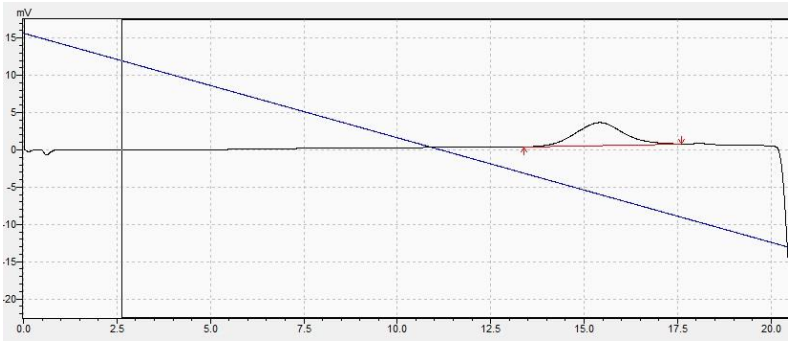

Figure S17. GPC trace for polymer product with $(CeLN"Br)_2$ (200:1, RT, 15 mins) as catalyst (Table 1, entry 6)

$(NdLN"Br)_2$

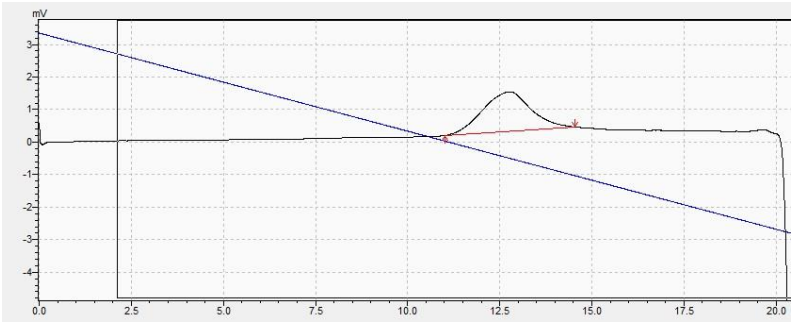

Figure S18. GPC trace for polymer product with $(NdLN"Br)_2$ (200:1, RT, 15 mns) as catalyst (Table 1, entry 7)

$LaLN"_2$

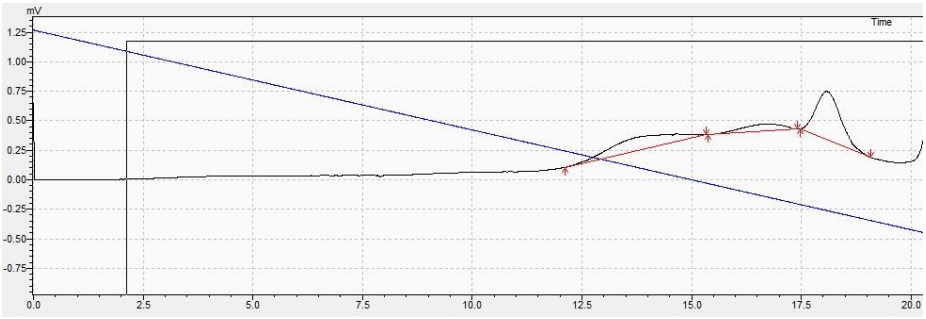

Figure S19. GPC trace for polymer product with $LaLN"_2$ (200:1, RT, 10 mins) as catalyst (Table 1, entry 9)

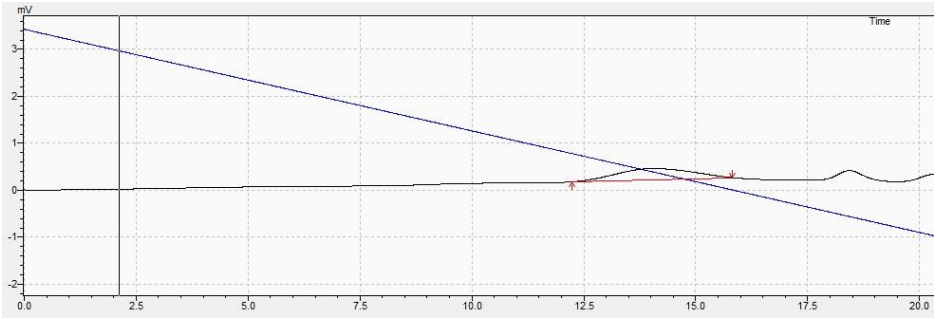

Figure S20. GPC trace for polymer product with $LaLN"_2$ (400:1, RT, 15 mins) as catalyst (Table 1, entry 10)

CeLN"$_2$

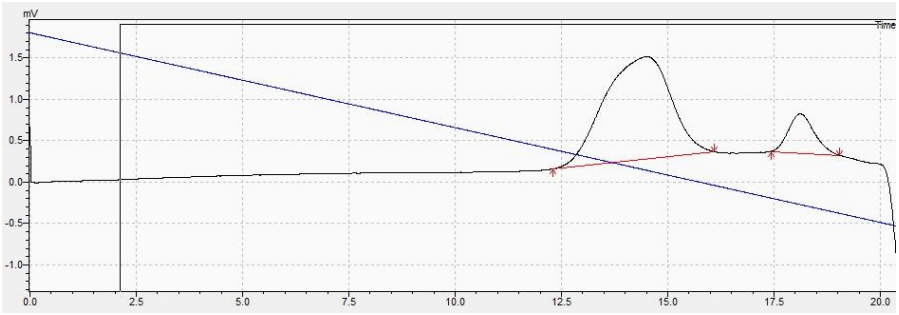

Figure S21. GPC trace for polymer product with CeLN"$_2$ (200:1, RT, 5 mins) as catalyst (Table 1, entry 11)

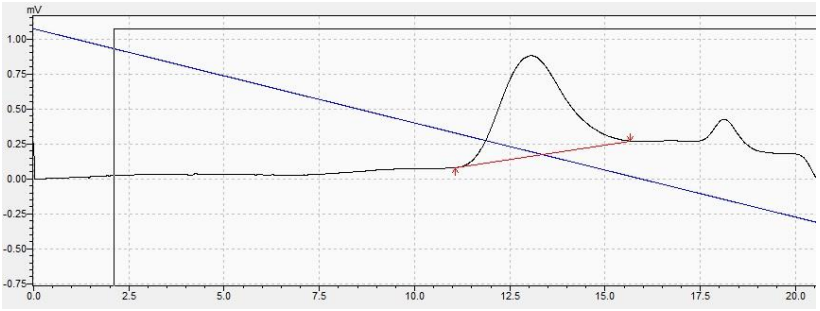

Figure S22. GPC trace for polymer product with CeLN"$_2$ (400:1, RT, 10 mins) as catalyst (Table 1, entry 12)

NdLN"$_2$

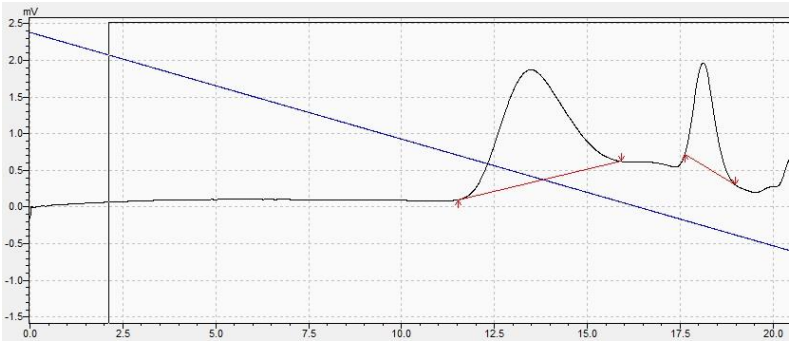

Figure S23. GPC trace for polymer product with NdLN"$_2$ (200:1, RT, 10 mins) as catalyst (Table 1, entry 13)

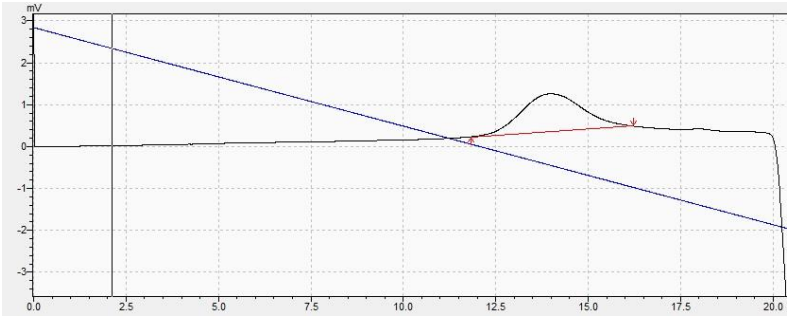

Figure S24. GPC trace for polymer product with NdLN"$_2$ (800:1, RT, 15 mins) as catalyst (Table 1, entry 14)

YTp$_2$N"

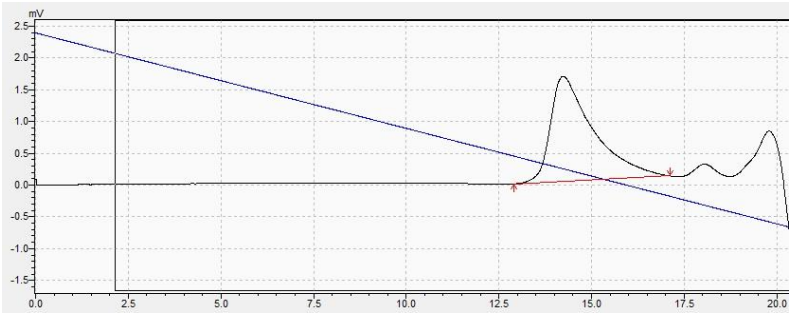

Figure S25. GPC trace for polymer product with YTp$_2$N" (200:1, 60 °C, 16 h) as catalyst (Table 1, entry 16)

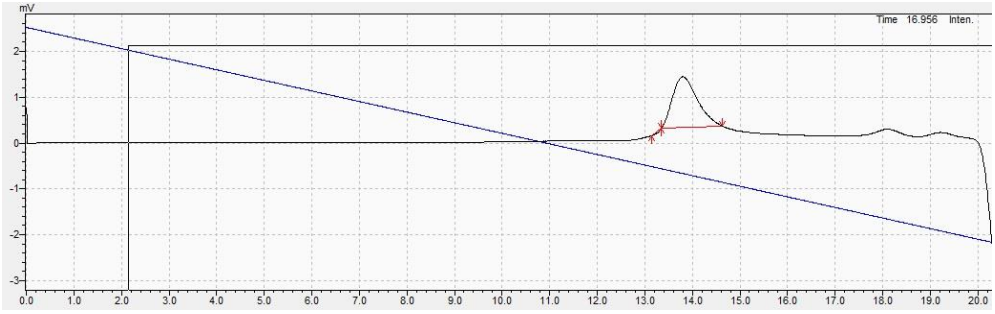

Figure S26. GPC trace for polymer product with YTp$_2$N" (400:1, 60 °C, 16 h) as catalyst (Table 1, entry 17)

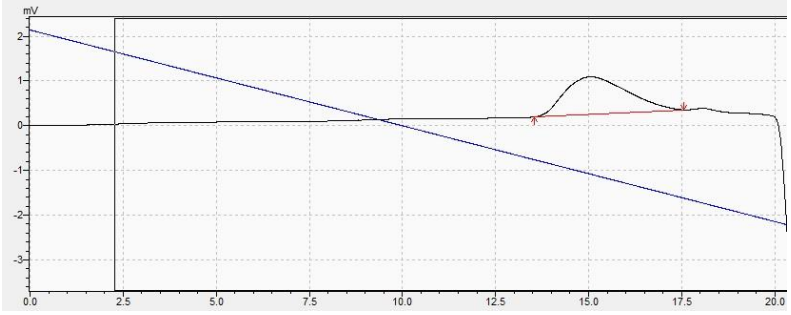

Figure S27. GPC trace for polymer product with YTp$_2$N" (800:1, 60 °C, 16 h) as catalyst (Table 1, entry 18)

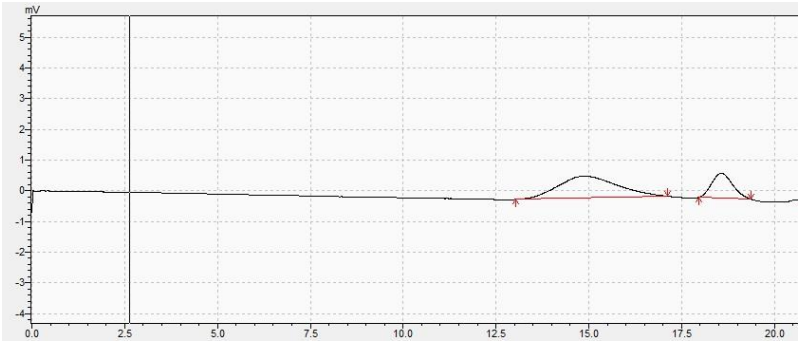

Figure S28. GPC trace for polymer product with YTp_2N" (200:1, 80 °C, 16 h) as catalyst (Table 1, entry 19)

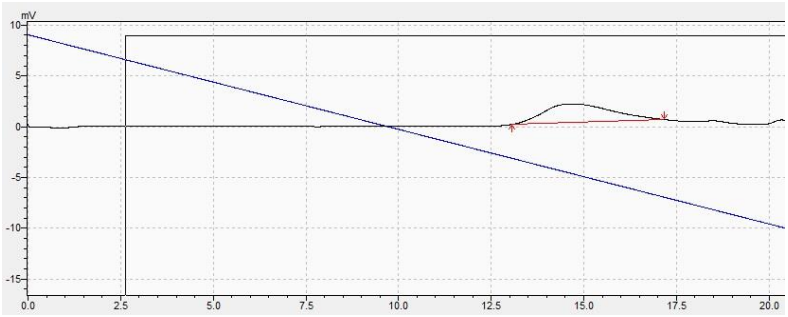

Figure S29. GPC trace for polymer product with YTp_2N" (400:1, 80 °C, 16 h) as catalyst (Table 1, entry 20)

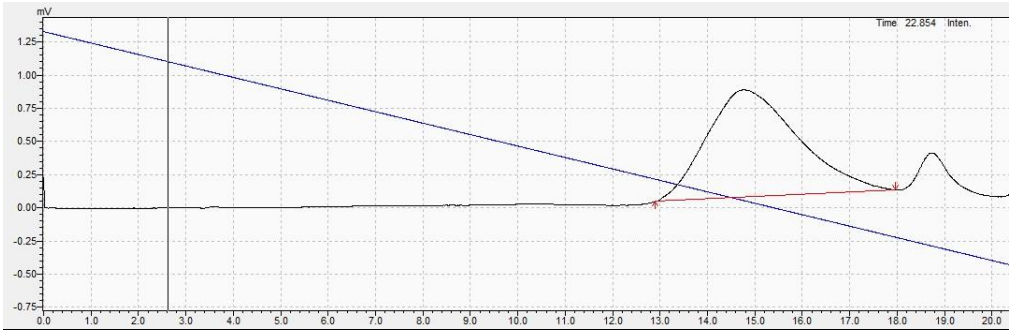

Figure S30. GPC trace for polymer product with YTp_2N" (800:1, 80 °C, 16 h) as catalyst (Table 1, entry 21)

X-Ray Crystallography

Crystallographic details

Single crystals suitable for x-ray diffraction were covered in inert oil and placed under the cold stream of a Bruker D8 Venture diffractometer at 100 K. Exposures were collected using Cu-K_a (l = 1.54178 Å). Indexing, data collection and absorption corrections were performed. The structures were then solved using SHELXT[6] and refined by full-matrix least-squares refinement (SHELXL)[5] interfaced with the programme OLEX2.[7]

The structures for all LnLN"$_2$ compounds (Ln = La, Ce and Nd in this paper, Ln = La in *P*-1 in a previous paper)[4] all feature large Q peaks next to the metal centres. This is despite crystallising in several different space groups (Ln = La in this paper: *Pca*2_1, Ln = Ce: *P*2_1/*c*, Ln = Nd: *Pca*2_1) and collecting several datasets. We have looked for non-merohedral twinning but have not been able to model the data any better than that presented here. We have used Cu radiation, which, although not ideal for heavy atoms, has worked satisfactorily with small crystals of other rare earth complexes (for example, the Ce Br bridged structure in this paper and the Nd Br bridged structure in a previous paper).[4] We are therefore unable to confirm whether the problem is exclusively absorption related or if the problem is inherent with the way this class of compounds crystallise. We present the data and draw conclusions only about the connectivity of the structures **5** – **7**.

Structure of fluorenyl-tethered ligand bromide proligand (**H_2LBr**)

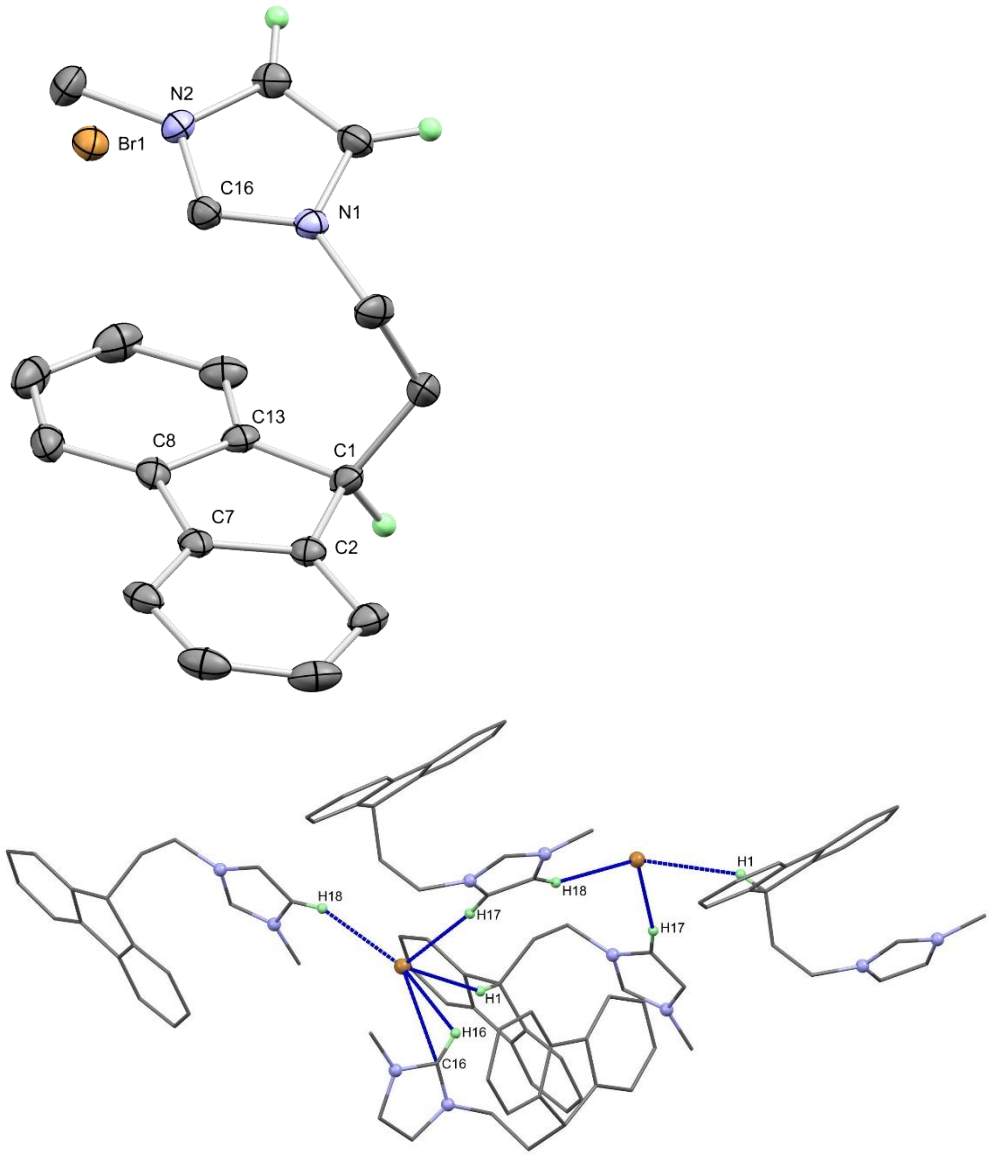

Figure S31. Molecular structure (top) and secondary interactions (bottom) of $[(C_{13}H_9)C_2H_4N(CH)C_2H_2N(Me)][Br]$ (**H_2LBr**) with thermal ellipsoids at 50% probability and all H atoms except for NHC backbone and Flu-H1 have been removed for clarity (top).

Structures of additional (bis)amide complexes

LaLN"$_2$ (**5**)

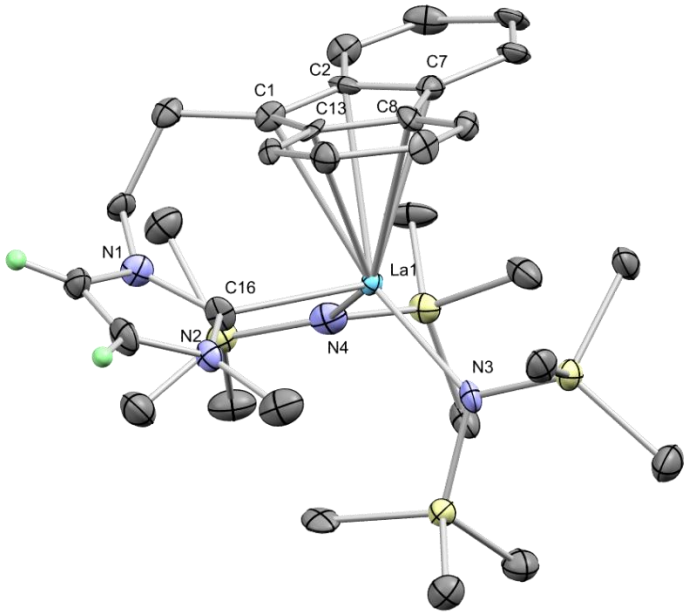

Figure S32. Molecular structure of LaLN"$_2$ (**5**) with thermal ellipsoids at 50% probability. All H atoms except for NHC backbone have been removed for clarity.

Table S1. Selected bond lengths (Å) and bond angles (°) for fluorenyl-tethered-NHC rare earth complexes.

Bond(s)	**1 (Y)**[a]	**3 (Ce)**	**4 (Nd)**[a]
Ln1-C1	2.6347(15)	2.845(2)	2.796(2)
Ln1-C2	2.6765(14)	2.928(2)	2.847(2)
Ln1-C7	2.6726(15)	2.949 (2)	2.869(2)
Ln1-C8	2.6676(15)	2.899 (2)	2.915(2)
Ln1-C13	2.6786(15)	2.884(2)	2.886(2)
Ln1-C16	2.4780(15)	2.676(2)	2.639(2)
Ln1-N3	2.2082(13)	2.3357(15)	2.3050(17
Ln1-N4	-	-	-
Ln1-Br1 Ln1-Br1'	2.7219(2)	2.9941(2) 3.0383(2)	2.9541(3) 3.0053(3)
Centroid-Ln-C16	103.5	93.3	94.2
C16-Ln-N3	100.63(5)	124.25(6)	122.21(7)
C16-Ln-N4	-	-	-
N3-Ln-N4	-	-	-

[a] Structure published previously.[4]

Table S2. Additional crystallographic data

	LH_2Br	**3** $\{CeL(Br)N''\}_2$
Empirical formula	$C_{19}H_{19}BrN_2$	$C_{50}H_{70}Br_2Ce_2N_6Si_4$
Formula weight	355.27	1307.54
T/K	100.0	100.0
Crystal system	orthorhombic	monoclinic
Space group	$P2_12_12_1$	$P2_1/n$
a/Å	11.1141(2)	11.4996(3)
b/Å	12.0398(3)	11.3835(3)
c/Å	12.4524(3)	21.0457(5)
α/°	90	90
β/°	90	95.4860(10)
γ/°	90	90
Volume/Å^3	1666.27(7)	2742.38(12)
Z	4	2
ρ_{calc}g/cm^3	1.416	1.583
μ/mm^1	3.329	15.494
F(000)	728.0	1308.0
Crystal size/mm^3	0.31 × 0.25 × 0.2	0.18 × 0.06 × 0.04
Radiation	CuK_α (λ = 1.54178)	CuK_α (λ = 1.54178)
2Θ range for data collection/°	10.22 to 144.37	8.44 to 144.278
Index ranges	-13 ≤ h ≤ 13, -14 ≤ k ≤ 13, -15 ≤ l ≤ 13	-14 ≤ h ≤ 14, -13 ≤ k ≤ 14, -25 ≤ l ≤ 24
Reflections collected	29705	30621
Independent reflections	3273 [R_{int} = 0.0305, R_{sigma} = 0.0170]	5386 [R_{int} = 0.0339, R_{sigma} = 0.0250]
Data/ restraints/ parameters	3273/0/200	5386/0/296
Goodness-of-fit on F^2	1.108	1.064
Final R indexes [I>=2σ (I)]	R_1 = 0.0196, $_wR_2$ = 0.0479	R_1 = 0.0191, $_wR_2$ = 0.0480
Final R indexes [all data]	R_1 = 0.0197, $_wR_2$ = 0.0480	R_1 = 0.0194, $_wR_2$ = 0.0481
Largest diff. peak/hole (e Å^{-3})	0.18/-0.33	0.74/-0.83
Flack parameter	-0.029(6)	N/A
CSD deposition numbers	2401175	2401176

Table S2 continued. Additional crystallographic data

	5 LaLN"$_2$	**6** CeLN"$_2$	**7** NdLN"$_2$
Empirical formula	$C_{31}H_{53}LaN_4Si_4$	$C_{31}H_{53}CeN_4Si_4$	$C_{31}H_{53}N_4NdSi_4$
Formula weight	733.04	734.25	738.37
T/K	100.0	100.0	100.0
Crystal system	orthorhombic	monoclinic	orthorhombic
Space group	*Pca*2$_1$	*P*2$_1$/*c*	*Pca*2$_1$
a/Å	12.9434(2)	18.1504(6)	12.9276(2)
b/Å	16.4994(2)	11.7451(4)	16.4136(3)
c/Å	16.8840(2)	19.4041(7)	16.8458(3)
α/°	90	90	90
β/°	90	116.065(2)	90
γ/°	90	90	90
Volume/Å^3	3605.72(8)	3715.8(2)	3574.48(11)
Z	4	4	4
ρ_{calc}g/cm^3	1.350	1.312	1.372
μ/mm^1	10.616	10.882	12.555
F(000)	1520.0	1524.0	1532.0
Crystal size/mm^3	0.181 × 0.167 × 0.149	0.17 × 0.16 × 0.04	0.18 × 0.08 × 0.03
Radiation	CuK$_\alpha$ (λ = 1.54178)	CuK$_\alpha$ (λ = 1.54178)	CuK$_\alpha$ (λ = 1.54178)
2Θ range for data collection/°	5.234 to 143.972	5.42 to 145.36	5.246 to 144.332
Index ranges	-15 ≤ h ≤ 15, -20 ≤ k ≤ 20, -20 ≤ l ≤ 20	-22 ≤ h ≤ 21, -14 ≤ k ≤ 13, -23 ≤ l ≤ 23	-15 ≤ h ≤ 15, -20 ≤ k ≤ 20, -20 ≤ l ≤ 20
Reflections collected	80345	90837	76590
Independent reflections	7433 [R_{int} = 0.0737, R_{sigma} = 0.0354]	7339 [R_{int} = 0.0685, R_{sigma} = 0.0282]	7357 [R_{int} = 0.0695, R_{sigma} = 0.0332]
Data/ restraints/ parameters	7433/13/377	7339/0/374	7357/1/377
Goodness-of-fit on F^2	1.058	1.062	1.018
Final R indexes [I>=2σ (I)]	R_1 = 0.0704, $_wR_2$ = 0.1775	R_1 = 0.0724, $_wR_2$ = 0.2005	R_1 = 0.0698, $_wR_2$ = 0.1775
Final R indexes [all data]	R_1 = 0.0765, $_wR_2$ = 0.1833	R_1 = 0.0770, $_wR_2$ = 0.2037	R_1 = 0.0730, $_wR_2$ = 0.1819
Largest diff. peak/hole (e Å^{-3})	9.96/-2.79	7.72/-1.60	6.37/-3.75
Flack parameter	*	N/A	*
CSD deposition numbers	2401177	2401178	2401179

* These were refined as two component twins, with relative ratios for **5** LaLN"$_2$ of 0.628(10) {Flack: 0.0014(19)} and 0.370(10) {Flack: 0.0008(19)} and for **7** NdLN"$_2$ of 0.858(7) {Flack: 0.0004(9)} and 0.142(7) {Flack: -0.0000(9)}.

APCI Mass spectrometry

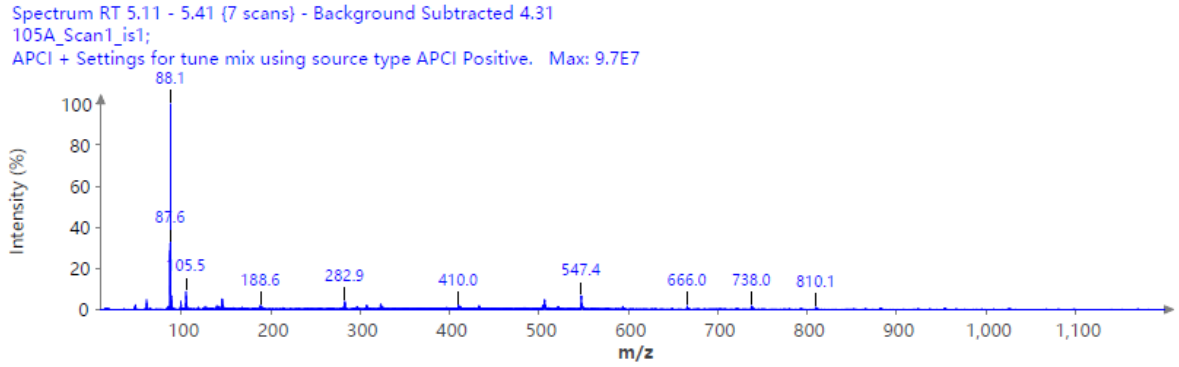

Figure S33. APCI Mass spectrum of polymer product from reaction of LaL_2Br (200:1, RT, 15 mins) as catalyst (Table 1, entry 5)

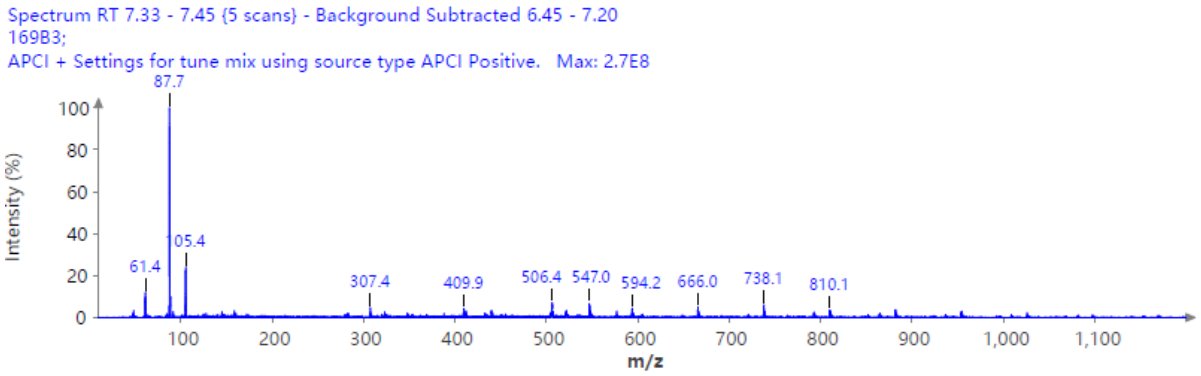

Figure S34. APCI Mass spectrum of polymer product from reaction of $NdLN"_2$ (200:1, RT, 10 mins) as catalyst (Table 1, entry 13)

References

1. P. Dubois, C. Jacobs, R. Jerome and P. Teyssie, *Macromolecules*, 1991, **24**, 2266-2270.
2. K. J. Evans, C. L. Campbell, M. F. Haddow, C. Luz, P. A. Morton and S. M. Mansell, *Eur. J. Inorg. Chem.*, 2019, **2019**, 4894-4901.
3. W. A. Herrmann and F. T. Edelmann, *Synthetic Methods of Organometallic and Inorganic Chemistry: Lanthanides and Actinides*, Thieme Medical Pub, 1996.
4. K. J. Evans, P. A. Morton, C. Sangster and S. M. Mansell, *Polyhedron*, 2021, **197**.
5. T. Chowdhury, S. J. Horsewill, C. Wilson and J. H. Farnaby, *Aust. J. Chem.*, 2022, **75**, 660-675.
6. G. Sheldrick, *Acta Crystallographica Section C*, 2015, **71**, 3-8.
7. O. V. Dolomanov, L. J. Bourhis, R. J. Gildea, J. A. K. Howard and H. Puschmann, *J. Appl. Crystallogr.*, 2009, **42**, 339-341.